

Reactive Transport Modeling of Mineral Precipitation Induced by Geomethanation[#]

Tianduoyi Wang¹, Keliu Wu^{1*}, Qingyuan Zhu¹, Zhe Hu¹, Zhangxin Chen^{1,2}

1 China University of Petroleum (Beijing), Beijing 102249, China

2 Department of Chemical and Petroleum Engineering, University of Calgary, Calgary T2N1N4, Canada

(Corresponding Author: wukeliu19850109@163.com)

ABSTRACT

Methanation is one of the most common microbial reactions in underground hydrogen storage (UHS). This biogeochemical reaction induces biofilm growth and mineral dissolution/precipitation, which in turn alter the reservoir pore structure and permeability, affecting the long-term multi-cycle operation of UHS systems. However, quantitative studies on biomass variation, the formation mechanism, spatiotemporal evolution, and key controlling factors of mineral precipitation during the injection and storage stages of UHS systems remain scarce. Based on PHREEQC software, this study developed a Darcy-scale reactive transport model integrating microbial reaction kinetics and mineral precipitation kinetics, followed by model validation. The model was used to analyze the spatiotemporal evolution characteristics of porosity during the hydrogen injection stage and the characteristics of UHS system parameters during the storage stage. The results show that mineral precipitation exhibits a heterogeneous distribution during the injection stage, and porosity is mainly influenced by mineral precipitation. During the storage stage, hydrogen consumption reaches its maximum after approximately 4.5 months, and the subsequent UHS system attains a stable state. This study provides a quantitative prediction tool for mineral precipitation in UHS systems and geo-methanation processes, and offers critical technical support for the site selection and evaluation of related projects.

Keywords: underground hydrogen storage, geomethanation, biofilm growth, mineral precipitation, reaction transport model

NONMENCLATURE

Abbreviations

UHS Underground Hydrogen Storage

Symbols

μ_{growth}	Microbial Growth Rate
$\mu_{\text{growth}}^{\text{max}}$	Maximum Growth Rate
C_{brine}	Molar Concentration of Components
k_{brine}	Half Saturation Constants for Each Substrate
γ	Microbial Death Rate
f_T	Rate correction factor caused by temperature
f_{pH}	Rate correction factor caused by pH
f_{TDS}	Rate correction factor caused by salinity
X_m	Total Number of Microorganisms in the Liquid Phase
v_m	The molar volume of microorganisms
S	Mineral reaction surface area
S_0	Initial surface area of mineral rocks
β	The power index of the reaction surface area and porosity of rocks
$\Delta \varepsilon_m$	Porosity changes caused by the growth of biofilms
$\Delta \varepsilon_c$	Porosity changes caused by mineral precipitation
L	Column length
A	Cross-sectional area of the column
R_p	Rate of calcite precipitation
k_1, k_2	Specific parameters of the mineral
α_{H^+}	Ion activity of H^+
$\alpha_{\text{CO}_3^{2-}}$	Ion activity of CO_3^{2-}
$\alpha_{\text{Ca}^{2+}}$	Ion activity of Ca^{2+}
v_D	Darcy velocity
Q	Darcy flow
α_L	Dispersion coefficient in porous media
r	Column radius
H	Column height
N	Number of grids
V_{cell}	Volume of the solution in each grid

1. INTRODUCTION

The global transition toward carbon neutrality has driven the rapid development of underground hydrogen storage (UHS) as a critical technology for addressing the intermittency of renewable energy and ensuring long-term energy security [1]. By injecting green hydrogen (H_2)—produced via electrolysis of water using surplus renewable electricity—into subsurface formations (e.g., depleted oil/gas reservoirs, deep aquifers), UHS enables large-scale, long-duration energy storage while aligning with low-carbon goals [2]. However, the subsurface environment is not a passive storage medium: native microbial communities in geological formations drive complex biogeochemical processes once H_2 is introduced, including biofilm growth, mineral dissolution, and mineral precipitation (e.g., calcite, hydroxides). These processes directly alter the reservoir's pore structure, permeability, and pore connectivity—key parameters governing H_2 injection efficiency, storage capacity, and the system's ability to operate safely over multiple cycles [3]. For instance, excessive mineral precipitation can clog pores and reduce injectivity, while biofilm accumulation may further modify fluid flow paths [4]; conversely, controlled mineralization could potentially enhance caprock integrity and prevent H_2 leakage. Thus, understanding and regulating these microbially mediated biogeochemical processes is essential to unlocking the full potential of UHS as a reliable energy storage solution.

Despite growing recognition of the importance of microbially induced processes in UHS, existing research still faces significant gaps and limitations. Most prior studies have focused on either macroscale UHS performance (e.g., storage capacity, injection rate) or laboratory-scale microbial metabolism, with limited integration of these two scales [5–8]. For example, laboratory microcosm experiments have confirmed that H_2 -utilizing microorganisms (e.g., methanogens) can induce mineral precipitation, but they fail to capture the spatial heterogeneity of pore structure changes or the dynamic interplay between fluid transport and biogeochemical reactions in real reservoirs. On the other hand, numerical models for UHS often simplify or overlook microbial processes, treating reservoirs as abiotic systems; while a few models incorporate microbial kinetics, they typically rely on commercial software (e.g., TOUGHREACT) with high computational costs, closed-source codes, and steep learning curves—limiting their accessibility and reproducibility [8,9]. Additionally, quantitative studies on how biofilm growth and mineral precipitation co-evolve across the two

critical stages of UHS (injection and storage) remain scarce, and the key factors controlling the spatial distribution of these processes (e.g., fluid flow, substrate availability) have not been systematically elucidated [10]. This disconnect between microscale biology and macroscale transport hinders the ability to predict reservoir behavior, optimize injection strategies, and mitigate risks (e.g., pore clogging) in practical UHS projects.

To bridge these gaps, this study develops a Darcy-scale one-dimensional reactive transport model using PHREEQC, an open-source geochemical software widely recognized for its flexibility in simulating biogeochemical reactions. The model is designed to explicitly integrate three core processes: (1) microbial kinetics; (2) biofilm dynamics; and (3) mineral precipitation/dissolution kinetics. The model simulates both the H_2 injection stage and the storage stage. This approach provides a low-cost, transparent, and reproducible tool to quantify microbially mediated biogeochemical processes in UHS, supporting the optimization of storage system design and risk assessment.

2. MODEL

The system studied in this paper comprehensively considers the fluid phase, three solid phases (rock, biofilm, and calcite), and dissolved components. Notably, calcite is adopted as the representative mineral precipitate in the model, as it is the dominant form of calcium carbonate. Herein, the biofilm refers to attached microorganisms capable of producing extracellular polymeric substances (EPS). Fig. 1 presents a pore-scale schematic of the studied system. All models constructed in this work are defined at the macroscale, with their rationality derived from the sufficient averaging of pore-scale processes.

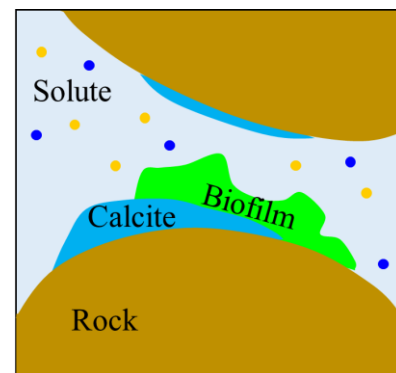


Fig. 1 Schematic diagram of pore-scale hydrogen storage system

2.1 Model assumption

For phase behavior and transport processes, the dissolution and desorption of gases such as H₂ and CH₄ at the gas-aqueous interface follow Henry's law, and their equilibrium constants can be adjusted using the Van't Hoff model when the temperature deviates from 25°C. Anhydrite, carbonate minerals, and biofilm are immobile phases, while suspended biomass and dissolved components migrate with the aqueous phase, and gas-phase components move with the gas phase. Key variables (e.g., component concentrations, phase saturation) are dynamically adjusted according to the presence and proportion of the gas and aqueous phases.

2.2 Chemical Reactions

2.2.1 Microbial Reaction Kinetics

For methanation reactions, the substrates include H₂ and HCO₃⁻, so the dual-Monod model can be used to represent the microbial growth rate:

$$\mu_{\text{growth}} = \mu_{\text{growth}}^{\max} \left(\frac{c_{\text{H}_2}}{k_{\text{brine}}^{\text{H}_2} + c_{\text{H}_2}} \right) \left(\frac{c_{\text{brine}}^{\text{HCO}_3^-}}{k_{\text{brine}}^{\text{HCO}_3^-} + c_{\text{brine}}^{\text{HCO}_3^-}} \right) \cdot f_T \cdot f_{\text{pH}} \cdot f_{\text{TDS}} \quad (1)$$

Considering that microbial reactions have an optimal temperature T_{opt} , an optimal pH value pH_{opt} , and an optimal salinity TDS_{opt} , and can only occur within a certain range of temperature, pH value, and salinity, the rate correction factors affected by temperature, pH value, and salinity can be expressed respectively as:

$$f_T = \begin{cases} \frac{(T - T_{\min})(T + T_{\min} - 2T_{\text{opt}})}{(T_{\text{opt}} - T_{\min})^2}, & T_{\min} < T < T_{\text{opt}} \\ 1, & T = T_{\text{opt}} \\ \frac{(T - T_{\max})(T + T_{\max} - 2T_{\text{opt}})}{(T_{\text{opt}} - T_{\max})^2}, & T_{\text{opt}} < T < T_{\max} \end{cases} \quad (2)$$

$$f_{\text{pH}} = \begin{cases} \frac{(\text{pH} - \text{pH}_{\min})(\text{pH} + \text{pH}_{\min} - 2\text{pH}_{\text{opt}})}{(\text{pH}_{\text{opt}} - \text{pH}_{\min})^2}, & \text{pH}_{\min} < \text{pH} < \text{pH}_{\text{opt}} \\ 1, & \text{pH} = \text{pH}_{\text{opt}} \\ \frac{(\text{pH} - \text{pH}_{\max})(\text{pH} + \text{pH}_{\max} - 2\text{pH}_{\text{opt}})}{(\text{pH}_{\text{opt}} - \text{pH}_{\max})^2}, & \text{pH}_{\text{opt}} < \text{pH} < \text{pH}_{\max} \end{cases} \quad (3)$$

$$f_{\text{TDS}} = \begin{cases} 1, & \text{TDS} < \text{TDS}_{\min} \\ \frac{(\text{TDS} - 2 \times \text{TDS}_{\min} + \text{TDS}_{\max})(\text{TDS}_{\max} - \text{TDS})}{(\text{TDS}_{\max} - \text{TDS}_{\min})}, & \text{TDS}_{\min} \leq \text{TDS} < \text{TDS}_{\max} \\ 0, & \text{TDS} > \text{TDS}_{\max} \end{cases} \quad (4)$$

The rate of change of biomass in the liquid phase can be expressed as:

$$\frac{dX_m}{dt} = \mu_{\text{growth}} X_m - \gamma X_m \quad (5)$$

The porosity change caused by the growth of biofilms can be expressed as:

$$\Delta \varepsilon_m = \frac{X_m v_m}{LA} \quad (6)$$

2.2.2 Mineral precipitation kinetics

During the process of mineral precipitation, the reaction surface area of rocks can be expressed as a function of porosity [11]:

$$S = S_0 \left(\frac{\varepsilon_0}{\varepsilon} \right)^\beta \quad (7)$$

The porosity change caused by mineral precipitation can be expressed as:

$$\Delta \varepsilon_c = \frac{R_p T v_c}{LA} \quad (8)$$

The rate of calcite precipitation is:

$$R_p = S(k_1 + k_2 \alpha_{\text{H}^+}) \left(1 - \frac{\text{IAP}}{K} \right) \quad (9)$$

$$\text{IAP} = \alpha_{\text{CO}_3^{2-}} \cdot \alpha_{\text{Ca}^{2+}} \quad (10)$$

2.3 Reactive transport model

Fig. 2 shows a one-dimensional reactive transport porous medium column. The column was initially filled with brine, which was in equilibrium with calcite and CO₂ gas phase, and there were stationary phase microorganisms attached to the surface of the porous medium rock. An aqueous solution containing H₂ was injected into the column to explore the dissolution/precipitation of calcite and the growth characteristics of biofilms along the direction of the column.

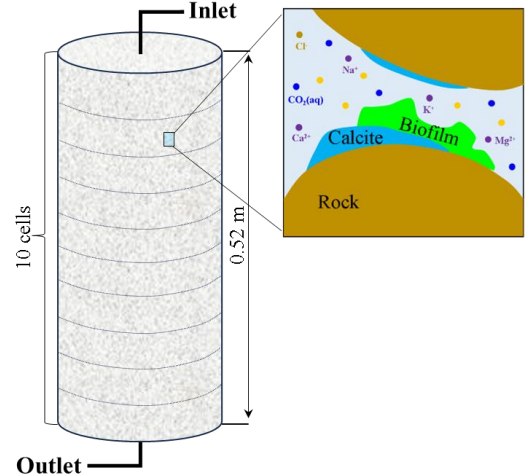


Fig. 2 A one-dimensional reactive transport porous medium column

Disperse the columns into 10 grid cells. Mineral precipitation and biofilm growth jointly occupy the pore space of porous media. Assuming that the volume fraction of the two is linearly and negatively correlated

with the effective porosity, the porosity evolution of each unit i caused by biofilm growth and mineral precipitation can be expressed as:

$$\varepsilon_i = \varepsilon_0 - \Delta\varepsilon_i^m - \Delta\varepsilon_i^c \quad (11)$$

In the column, the fluid flow rate is expressed as:

$$v_D = \frac{Q}{A} \quad (12)$$

Dispersion in porous media is used to quantify the mechanical dispersion effect that occurs when solutes migrate in porous media, and is defined as:

$$\alpha = \frac{D_L}{v_D} \quad (13)$$

Table 1 shows the basic input parameters of the reaction transfer model of the hydrogen storage reservoir in the aquifer. The solution domain is meshed, and the volume of the solution in each grid is:

$$V_{\text{cell}} = \frac{\pi r^2 H \varphi_0}{N} \quad (14)$$

Table 1 Input parameters of the reactive transport model

Category	Parameter	Value
Flow parameters	Flow rate	$4 \cdot 10^{-5}$ l/s
	Stage I	Injection
	Stage II	Storage
	Duration of stay	10 hours
	Pore volume injected	1.5 PV
	Boundary condition	Flux, Constant
Microbial parameters	Microbial Growth Rate μ_{max}	1.109/day
	Initial microbial quantity	cells/mL
	Microbial decay coefficient γ	$0.01 \mu_{\text{max}}/\text{day}$
	Yield coefficient	0.03 molX/molH_2
	$T_{\text{min}}, T_{\text{max}}, T_{\text{opt}}$	10, 122, 45 °C
	$\text{pH}_{\text{min}}, \text{pH}_{\text{max}}, \text{pH}_{\text{opt}}$	4.1, 10.2, 7.7
	$\text{TDS}_{\text{min}}, \text{TDS}_{\text{max}}$	50, 300
Brine component	Chloride	19773 ppm
	Sodium	10890 ppm
	Magnesium	1368 ppm
	Sulfate	2960 ppm
	Calcium	428 ppm
Rock	Potassium	460 ppm
	initial porosity	0.35
	Soil height	55 cm
	Particle size	0.21 mm

2.4 Model validation

Experimental data were used to validate the model [12]. Fig. 3 shows the concentration distribution of calcite precipitation along the column. The results demonstrate that the constructed microbially induced mineral precipitation model is in good agreement with

the experimental data, confirming the model's reliability. Additionally, a grid independence test was performed to verify numerical stability.

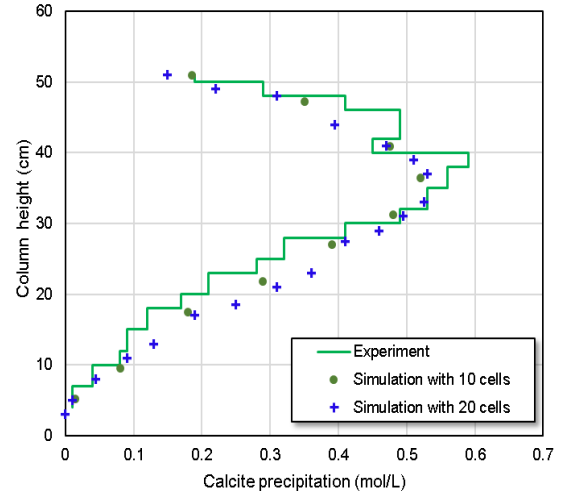


Fig. 3 Model validation

3. RESULTS AND DISCUSSION

3.1 Injection stage

Fig. 4 shows the distribution profile of porosity, H_2 consumption, calcite precipitation and biomass increase along the column at 8900 seconds of injection. The results indicate that during H_2 injection, porosity, H_2 consumption, biomass, and calcite moles exhibit significant heterogeneous distributions along the reaction column depth, with the most pronounced effects observed at Grid 9 (i.e., 0.468 m from the injection point). Porosity shows a gradient distribution characterized by "stability in the upper-middle section and sharp attenuation at the bottom":

- Porosities at Nodes 1–7 remain 0.379–0.380 (deviation from the initial value < 0.3%), unaffected by significant precipitation;
- Porosity at Node 8 decreases to 0.377 (0.8% reduction), serving as a reaction transition interface;
- Porosities at Nodes 9–10 (especially Node 9) drop sharply to 0.361–0.367 (3.4%–5.0% reduction), representing the core calcite precipitation zone.

This phenomenon arises because initial precipitation at the bottom fills pores, increasing seepage resistance and extending the local residence time of H_2 and ions. This further promotes microbial metabolism and mineral precipitation, ultimately leading to rapid pore clogging at the bottom.

3.2 Storage stage

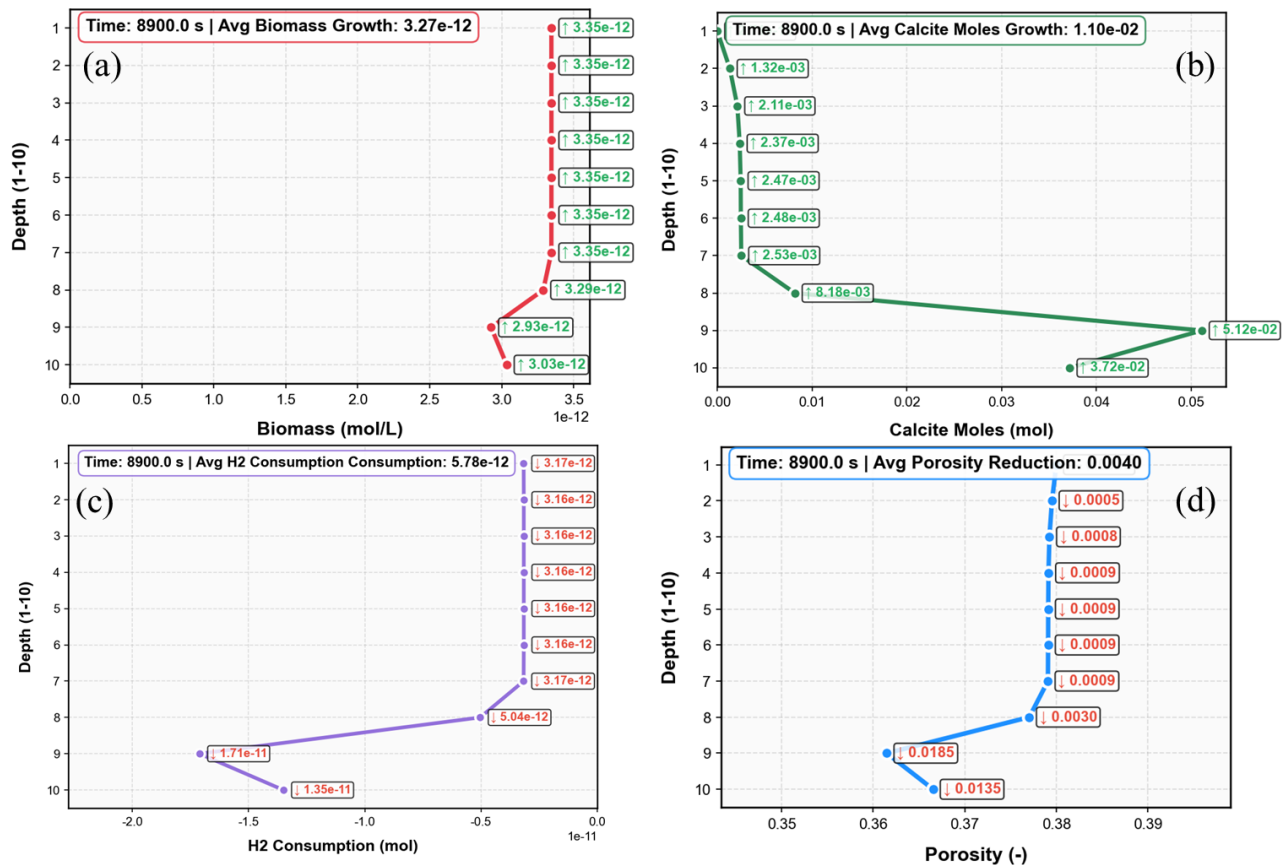


Fig. 4 Column parameter characteristics at the post-injection stage

Fig. 5 presents the continuous response patterns of substrate consumption, biomass dynamics, gas products, and environmental parameters in the hydrogenotrophic methanation system, whose metabolic process can be divided into three stages: rapid proliferation, stable

metabolism, and decay equilibrium. During the rapid proliferation stage (0~137 d), H₂ is rapidly consumed as the core electron donor (Fig. 5a), and its consumption approaches saturation at 137 d—confirming its role as the limiting substrate for methanation. Synchronously,

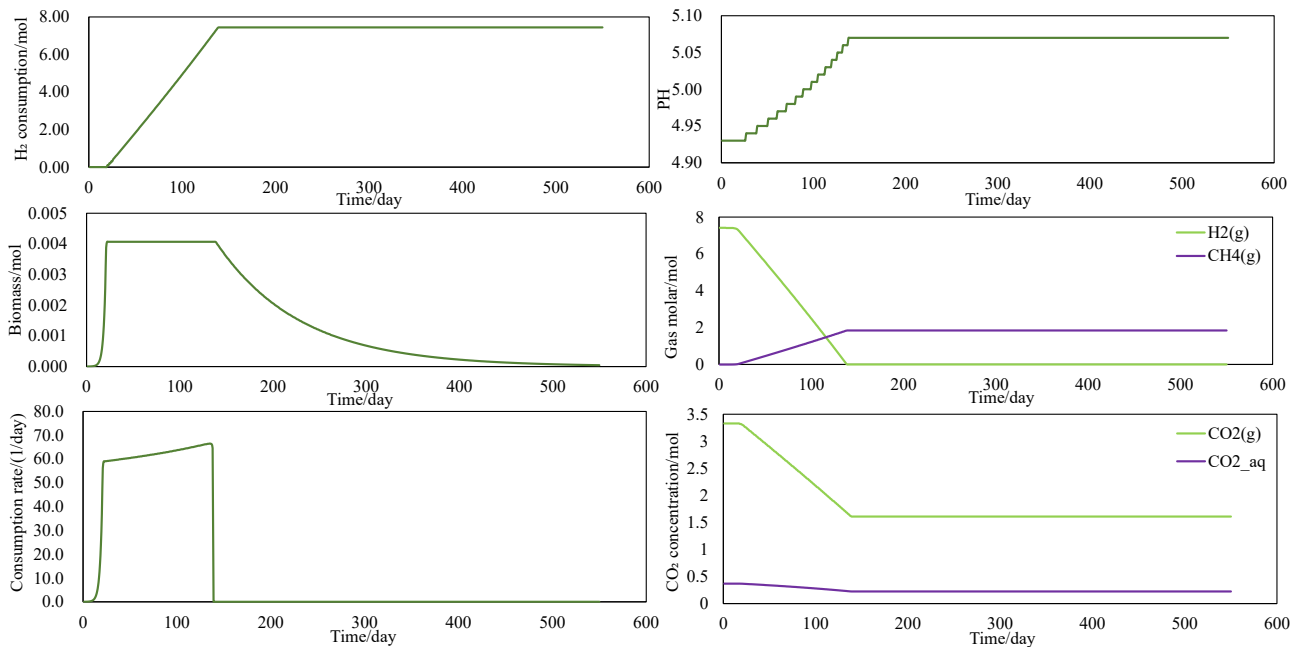


Fig. 5 Dynamic characteristics of parameters in the hydrogen storage stage

microbial biomass undergoes explosive growth (Fig. 5c), reflecting the high proliferation activity of hydrogenotrophic methanogens under substrate-sufficient conditions. Sustained methanogenic metabolism during this stage gradually increases the system pH from an initial 4.5 to 5.05 (Fig. 5b), attributed to H^+ consumption and accumulation of weakly alkaline metabolites (e.g., HCO_3^-), with the pH eventually stabilizing within the optimal physiological range (5.0~7.5) for methanogens. Among gas products, $CH_4(g)$ is generated synchronously with H_2 consumption (Fig.5d), while the concentration of $CO_2(g)$ decreases rapidly (Fig. 5f); $CO_2(aq)$ remains at a low level throughout, indicating that part of the CO_2 dissolves in the brine and participates in the reaction.

4. CONCLUSIONS

In this study, a one-dimensional reactive transport model was constructed to systematically simulate the hydrogenotrophic methanation process and its induced calcite precipitation in deep aquifers. The main conclusions are as follows:

(1) Injection stage: During H_2 injection, significant pore clogging occurs at the bottom of the reaction column, with a maximum porosity reduction of 5.0%. This indicates that injection methods need to be optimized in practical engineering to mitigate local clogging risks.

(2) Storage stage: The system undergoes three stages: rapid proliferation, stable metabolism, and decay equilibrium. As the limiting substrate, H_2 is rapidly consumed within 137 days, microbial biomass increases significantly, the pH value rises from 4.5 to 5.05 and stabilizes within the optimal range, and CH_4 generation proceeds synchronously with CO_2 consumption.

(3) Model reliability: The model-predicted calcite precipitation distribution is in good agreement with experimental data. The grid independence test confirms the stability and reliability of the numerical results, validating the model's applicability in describing microbe-mineral-fluid interactions.

This study provides a systematic simulation framework for biogeochemical processes during underground hydrogen storage, facilitating an in-depth understanding of the mechanism of microbially induced mineral precipitation and its impacts on reservoir properties. It offers theoretical support and a tool reference for the implementation and risk management of future underground hydrogen storage projects.

ACKNOWLEDGEMENT

This work was supported by National Natural Science Foundation of China [No.52174041].

REFERENCE

- [1] Jafari Raad SM, Leonenko Y, Hassanzadeh H. Hydrogen storage in saline aquifers: Opportunities and challenges. *Renewable and Sustainable Energy Reviews* 2022;168:112846. <https://doi.org/10.1016/j.rser.2022.112846>.
- [2] Edlmann K. Challenging perceptions of underground hydrogen storage. *Nat Rev Earth Environ* 2024;5:478–80. <https://doi.org/10.1038/s43017-024-00572-8>.
- [3] Gao Q. Phenomenal study of microbial impact on hydrogen storage in aquifers: A coupled multiphysics modelling. *International Journal of Hydrogen Energy* 2024.
- [4] Ebigbo A, Phillips A, Gerlach R, Helmig R, Cunningham AB, Class H, et al. Darcy-scale modeling of microbially induced carbonate mineral precipitation in sand columns. *Water Resources Research* 2012;48:2011WR011714. <https://doi.org/10.1029/2011WR011714>.
- [5] Wang G, Pickup G, Sorbie K, De Rezende JR, Zarei F, Mackay E. Bioreaction coupled flow simulations: Impacts of methanogenesis on seasonal underground hydrogen storage. *International Journal of Hydrogen Energy* 2024;55:921–31. <https://doi.org/10.1016/j.ijhydene.2023.11.035>.
- [6] Minougou JD, Azizmohammadi S, Gholami R, Ott H. A bio-reactive transport model for biomethanation in hydrogen underground storage sites. *Greenhouse Gases* 2024;14:977–94. <https://doi.org/10.1002/ghg.2307>.
- [7] Liu Y, Li HA, Okuno R. Measurements and modeling of interfacial tension for CO_2/CH_4 /brine systems under reservoir conditions. *Ind Eng Chem Res* 2016;55:12358–75. <https://doi.org/10.1021/acs.iecr.6b02446>.
- [8] Bhukya PK, Adla N, Arnepalli DN. Coupled bio-chemo-hydro-mechanical modeling of microbially induced calcite precipitation process considering biomass encapsulation using a micro-scale relationship. *Journal of Rock Mechanics and Geotechnical Engineering* 2024;16:2775–89. <https://doi.org/10.1016/j.jrmge.2023.09.023>.
- [9] Wang X, Nackenhorst U. Micro-feature-motivated numerical analysis of the coupled bio-chemo-hydro-mechanical behaviour in MICP. *Acta Geotech* 2022;17:4537–53. <https://doi.org/10.1007/s11440-022-01544-2>.
- [10] Liu N, Ostertag-Henning C, Fernø MA, Dopffel N. Growth on hydrogen by the sulfate-reducing

oleidesulfovibrio alaskensis induces biofilm dispersion and detachment—implications for underground hydrogen storage. Environ Sci Technol 2025;59:7095–105. <https://doi.org/10.1021/acs.est.4c13893>.

[11] Razbani MA, Røyne A, Jettestuen E. A One-Dimensional Reactive Transport Model for Microbially Induced Calcium Carbonate Precipitation (MICP) in Phreeqc. Geomicrobiology Journal 2025;42:19–29. <https://doi.org/10.1080/01490451.2024.2425295>.

[12] Martinez BC, DeJong JT, Ginn TR, Montoya BM, Barkouki TH, Hunt C, et al. Experimental Optimization of Microbial-Induced Carbonate Precipitation for Soil Improvement. J Geotech Geoenviron Eng 2013;139:587–98. [https://doi.org/10.1061/\(ASCE\)GT.1943-5606.0000787](https://doi.org/10.1061/(ASCE)GT.1943-5606.0000787).